ACS Catalysis

Research Article

pubs.acs.org/acscatalysis

Reaction Mechanism for Direct Propylene Epoxidation by Alumina-Supported Silver Aggregates: The Role of the Particle/Support Interface

Lei Cheng,[†] Chunrong Yin,[†] Faisal Mehmood,[‡] Bin Liu,[§] Jeffrey Greeley,[§,∥] Sungsik Lee,[⊥] Byeongdu Lee,[⊥] Sönke Seifert.,[⊥] Randall E. Winans,[⊥] Detre Teschner,[⊗] Robert Schlögl,[⊗] Stefan Vajda,[†,§,○] and Larry A. Curtiss*[,†,§]

[†]Materials Science Division, [§]Center for Nanoscale Materials, and [⊥]X-ray Sciences Division, Argonne National Laboratory, Argonne, Illinois 60439, United States

[‡]Air Force Research Laboratory, Materials& Manufacturing Directorate, Wright-Patterson Air Force Base, Ohio 45433, United States

[∥]School of Chemical Engineering, Purdue University, West Lafayette, Indiana 47907, United States

[⊗]Abteilung Inorganische Chemie, Fritz-Haber-Institut, D-14915 Berlin, Germany

[○]Department of Chemical and Environmental Engineering, Yale University, 9 Hillhouse Avenue, New Haven, Connecticut 06520, United States

Supporting Information

ABSTRACT: Subnanometer Ag aggregates on alumina supports have been found to be active toward direct propylene epoxidation to propylene oxide by molecular oxygen at low temperatures, with a negligible amount of carbon dioxide formation (*Science* **2010**, *328*, 224,). In this work, we computationally and experimentally investigate the origin of the high reactivity of the subnanometer Ag aggregates. Computationally, we study O_2 dissociation and propylene epoxidation on unsupported Ag_{19} and Ag_{20} clusters, as well as alumina-supported Ag_{19}. The O_2 dissociation and propylene epoxidation apparent barriers at the interface between the Ag aggregate and the alumina support are calculated to be 0.2 and 0.2−0.4 eV, respectively. These barriers are somewhat lower than those on sites away from the interface. The mechanism at the interface is similar to what was previously found for the silver trimer on alumina and can account for the high activity observed for the direct oxidation of propylene on the Ag aggregates. The barriers for oxygen dissociation on these model systems both at the interface and on the surfaces are small compared to crystalline surfaces, indicating that availability of oxygen will not be a rate limiting step for the aggregates, as in the case of the crystalline surfaces. Experimentally, we investigate Ultrananocrystalline Diamond (UNCD)-supported silver aggregates under reactive conditions of propylene partial oxidation. The UNCD-supported Ag clusters are found to be not measurably active toward propylene oxidation, in contrast to the alumina supported Ag clusters. This suggests that the lack of metal-oxide interfacial sites of the Ag-UNCD catalyst limits the epoxidation catalytic activity. This combined computational and experimental study shows the importance of the metal-oxide interface as well as the noncrystalline nature of the alumina-supported subnanometer Ag aggregate catalysts for propylene epoxidation.

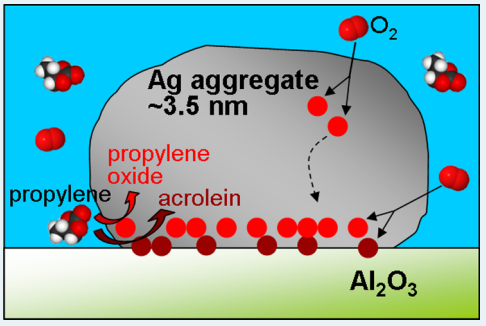

KEYWORDS: *propylene epoxidation, silver aggregates, density functional theory, grazing incidence X-ray scattering, assembly of size-selected clusters, temperature programmed reaction, X-ray absorption, interface*

1. INTRODUCTION

Propylene oxide (PO) is a key precursor of great value to the chemical industry. However, current industrial production methods of PO are either environmentally unfriendly or not very economical. The direct partial oxidation of propylene by molecular oxygen is a potential method for production of PO, but an efficient catalyst for this reaction is yet to be identified.[1−7] Silver has long been used as an industrial catalyst for the epoxidation reaction of ethylene,[2,8] but silver surfaces have very poor selectivity for the epoxidation reaction of propylene.[3,4,6,7,9] The reaction mechanisms, thermodynamics, and kinetics of ethylene or propylene epoxidation on silver crystal surfaces have previously been studied computationally.[10−14] Model silver clusters with sizes between 9 to 23 nm were recently investigated for their size-dependent catalytic performances for propylene epoxidation.[15] However, because these particles expose mainly crystal surfaces, the reactivity of these clusters is still dominated by that of the crystal surfaces. In contrast, in a study[16] of alumina-supported Ag trimers and

Received: June 3, 2013
Published: November 21, 2013

   dx.doi.org/10.1021/cs4009368 | *ACS Catal.* 2014, 4, 32−39

aggregates with diameters under ~3.5 nm, the silver particles were found to be very active for the direct propylene epoxidation to PO by molecular oxygen at low temperatures, with a negligible amount of carbon dioxide formation. However, much is unknown about the actual catalytic mechanisms on these small silver aggregates.

The supported subnanometer trimers and their aggregates are characterized by noncrystalline surfaces and interfacial sites with the support that are not present in the catalysts based on crystalline surfaces. In our previous work, first principles density functional theory (DFT) calculations were used to investigate the propylene epoxidation reaction on a supported Ag trimer.[16] Herein, we study O_2 dissociation and propylene epoxidation on catalytic sites of larger unsupported Ag clusters, Ag_{19} and Ag_{20}, as well as Ag_{19} with an alumina support using density functional calculations as models for investigating the activity of the aggregates and the support effect. The purpose of the work reported here is to compare the propylene epoxidation catalytic reaction mechanisms on the aggregates to that on Ag crystalline surfaces and the Ag trimers. One of the key questions for these calculations is whether the interface sites for the aggregates have similar catalytic properties as was identified for the trimer. In the case of the trimer, the silver interface oxygen was found to be very effective for PO formation, and the alumina surface interface oxygen was effective for acrolein formation.[16] Another key question is whether oxygen dissociation is rate limiting, as in the case of Ag crystalline surfaces.[14] We also report new experimental studies of silver aggregates on a diamond support to further understand the role of the interface sites in the PO catalysis mechanism, since diamond is likely to have a small support effect.

2. METHODS

Theoretical Methods. The initial structures of the Ag_{19} and Ag_{20} clusters were truncated from the Ag bulk. The initial structure of the hydroxylated amorphous alumina model was obtained from a molecular dynamics (MD) simulation using the same methodology described in previous studies.[17,18] The MD box has a dimension of $a = b = 11$ Å and $c = 80.52$ Å with H content of 8% and a total of 97 atoms. The structure from the MD simulation was then used for DFT calculations. The unit cell of the amorphous alumina used for DFT calculations was constructed by doubling the MD cell in the surface dimension and reducing the vacuum space in the c dimension to 10 Å. It has a dimension of $a = b = 15.56$ Å and $c = 20$ Å and contains a total of 194 atoms. On the hydroxylated amorphous alumina surface, aluminum cations have either four- or five- fold coordination, and oxygen atoms have either two- or three- fold coordination. These coordination numbers are consistent with theoretical and experimental results reported in literature for bulk amorphous alumina.[19−21]

All structures and energies were calculated using the PW91 DFT method[22] with plane-wave basis sets as implemented in VASP.[23−26] All calculations performed are spin-polarized. The core electrons were described by the ultrasoft pseudopotentials with cutoff energies of 400 eV for all atoms. The Γ-point and a $2 \times 2 \times 1$ k-point mesh were used to sample the Brillouin zones in the gas phase cluster and alumina-supported cluster calculations, respectively. In cluster calculations, all atoms were allowed to relax; in the alumina-supported cluster calculations, atoms in the bottom half of the alumina slab were kept frozen while those on top of the alumina slab, along with silver atoms and reactant molecules, were allowed to relax. The climbing image nudged elastic band (NEB) method was used to locate transition states. Each transition state was confirmed to have only one imaginary vibrational mode through explicit frequency calculation.

Experimental Section. Size-selected Ag_3 clusters were soft-landed on a doped silicon chip coated with ultrananocrystalline diamond (UNCD) film, under identical deposition and coverage conditions and surface coverage (corresponding to 2.2% ML of an ideal smooth surface) as in the case of the alumina support reported earlier.[16] The silicon wafers coated with UNCD particles were purchased from Advanced Diamond Technologies (UNCD, 25 Aqua DoSi)[27] and the deposited UNCD is 300 nm thick. The deposition of size-selected cluster was described in detail elsewhere.[16,28] Briefly, the molecular beam of silver clusters was produced by laser vaporization of a silver target using helium as carrier gas. Next, the beam was guided through an ion optics and quadrupole assembly, and the mass-selected positively charged cluster ions were soft-landed on the support. The amount of deposited metal was determined by real-time monitoring of the deposition flux.

The assembly of the Ag_3 clusters on UNCD was monitored by in situ GISAXS at the 12-ID-B beamline of the Advance Photon Source of Argonne National Laboratory, under a gas mixture consisting of C_3H_6:O_2:He = 0.67:0.33:99, using the same in situ cell, to warrant identical reaction conditions as in the previous report on the alumina-supported Ag_3 clusters.[16] The reaction products were analyzed on a differentially pumped quadrupole mass spectrometer (Pfeiffer). The GISAXS data were collected on a 1475 × 1679 pixel Pilatus 2 M detector with X-rays of 12 keV. The sample was placed on a ceramic heater (Momentive Performance Materials), and the temperature was programmed using a Lakeshore 340 controller. Further details can be found elsewhere.[16,28−33] The size distribution of silver particles at 200 and 500 °C was determined by using Irena SAS data analysis package.[34] The scattering at elevated temperatures was fit with two populations. One was assigned to the same population as obtained from fitting the scattering from the blank UNCD support, while the other was considered to be from silver particles. Two poly disperse spherical particle models, where the Schultz function is used as the size-distribution function, are employed to fit the data and separate the information of Ag particles from the roughness of UNCD. The results for Ag_3 particles on UNCD are compared to the Ag_3 aggregates on alumina supports studied in our previous work.[16]

3. RESULTS AND DISCUSSION

3.1. Computational Section. Detailed DFT calculations of a 3 nm Ag aggregate are computationally prohibitive, but models of smaller clusters can mimic under-coordinated surface features present on these aggregates. We have therefore used Ag_{19} and Ag_{20} clusters in our calculation as models for the ~3 nm Ag aggregates, studied experimentally in previous work on alumina[16] and in this work on UNCD. The results for the two aggregates should be representative since, like the supported Ag aggregates, Ag_{19} and Ag_{20} expose a variety of sites and have substantial interfacial area with the support, allowing for investigations of the geometric and support effects on reactivity. With the subnanometer clusters being amorphous, the clusters will present an ensemble of various sites with different reactivities. Although the combinations of surface sites might change with the size of the clusters, such variation is difficult to predict, and particle sizes are not explicitly sampled in the

dx.doi.org/10.1021/cs4009368 | ACS Catal. 2014, 4, 32−39

current work. Rather, our focus is to compare unsupported and supported clusters to emphasize the role of the cluster/support interface. In addition, Ag_{19} has one unpaired electron in its ground state (doublet) while Ag_{20} has a closed-shell structure (singlet), so the comparison between the two will provide some insight into spin effects on the reactivity of Ag aggregates.

3.1.1. O_2 Dissociation on Unsupported Ag_{19} and Ag_{20} Clusters. The Ag_{19} and Ag_{20} clusters have several geometrically equivalent facets and sites as indicated in Figure 1: the

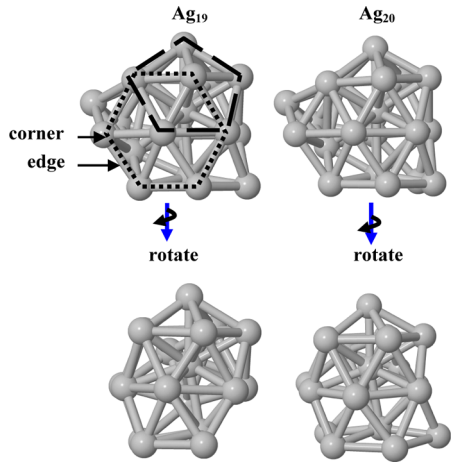

Figure 1. Two different views of the optimized structures of the (a) Ag_{19} and (b) Ag_{20} clusters. Note that similar pentagonal pyramid and hexagon facets (indicated by dotted and dashed lines, respectively), as well as corner and edge sites, are exhibited on both structures.

pentagonal pyramid-like and hexagon-like facets, as well as corner and edge sites. We investigated O_2 dissociation on these sites of the two clusters. The Ag_{19} cluster has a doublet ground state. We assume that the spin of the Ag_{19} pairs up with one spin from the triplet ground state of the oxygen molecule; thus, the O_2 dissociation reaction proceeds on a doublet potential energy surface (PES), and all reaction energies and barriers as reported in Table 1 are for doublet Ag_{19}. The pentagonal

Table 1. Barriers and Reaction Energies (in eV) of O_2 Dissociation on Various Sites of the Ag_{19} and Ag_{20}[a]

	Ag_{19}		Ag_{20}	
	E_{act}	ΔE	E_{act}	ΔE
PP neighbor	0.46	−0.35	0.74	0.04
PP non-neighbor	1.10	−1.21	0.99	−1.16
hexagon	0.57	−1.05	0.66	−1.19
edge	0.81	0.14	0.97	−0.04
corner	2.60	−1.03		

[a]Energies are calculated relative to the gas phase silver cluster and O_2 molecule.

pyramid facet was found to be present on most silver clusters in the size range of 7 to 21 atoms in a previous computational study.[35] The barriers for O_2 dissociation on this facet either to two neighboring hollow sites ("PP neighbor") or to two non-neighboring hollow sites ("PP non-neighbor") on Ag_{19} were calculated to be 0.44 and 1.10 eV (Table 1), respectively, relative to the sum of energies of a gas phase O_2 molecule and the Ag_{19} cluster (see Supporting Information, Figure S1 for structures). The barriers for O_2 dissociation on the hexagonal facet to two non-neighboring hollow sites ("Hexagon"), as well as on the edge ("Edge") and corner ("Corner") of the Ag_{19}, were calculated to be 0.57, 0.81, and 2.60 eV, respectively (see Supporting Information, Figure S1 for structures).

The O_2 dissociation reaction on Ag_{20} starts with a triplet state (a triplet O_2 and a singlet Ag_{20}). However, after O_2 adsorption, all intermediate structures have lower energies in the singlet state than the triplet, so we assume a curve crossing from the triplet to the singlet PES occurs during O_2 adsorption. Therefore, all barrier and reaction energies for Ag_{20} we calculated are energies on the singlet PES relative to the triplet gas phase O_2 and singlet Ag_{20} (see Table 1). Comparing the barriers of the Ag_{20} cluster with Ag_{19}, we find that the "PP non-neighbor" barrier of the Ag_{20} is lower than its counterparts on Ag_{19}, while those of the other three sites ("PP neighbor", "Hexagon" and "Edge") are higher than on Ag_{19}. Nevertheless, the differences in barriers between equivalent sites of the two clusters are small (less than 0.3 eV). Therefore, the comparison of the two clusters results suggests that the spin effect does not have a major impact on O_2 dissociation kinetics. However, the barriers of different sites on the same cluster vary significantly. This indicates that O_2 dissociation activity is highly site-dependent. For both clusters, O_2 dissociation barriers on "PP neighbor" and "Hexagon" are much lower than that on a Ag(111) surface (1.19 eV, calculated with O_2 coverage of 0.33 monolayer). This indicates that if small subnanometer clusters expose such sites ("PP neighbor" and "Hexagon") on the support, they are likely to be more active for O_2 dissociation than on larger nanometer clusters (>9 nm) on which the (111) surface is dominant.[15]

After O_2 dissociation, the two O atoms located at two non-neighboring 3-fold hollow sites are thermodynamically more favorable than if located at two neighboring sites, as the comparison of the relative energies and structures of the O_2 dissociation products in Supporting Information, Figure S1 shows. If two oxygen atoms are in neighboring sites on the Ag aggregate after O_2 dissociation, one can migrate to a non-neighboring site, and the migration is thermodynamically downhill and only corresponds to a small barrier of 0.1−0.2 eV (Supporting Information, Figure S2). Therefore, we assume that after O_2 dissociation, diffusion of one O from a neighboring to a non-neighboring site will occur unless the oxygen coverage is very high. Consequently, we used a structure with two oxygen atoms in two non-neighboring sites as the starting point for the investigation of the propylene oxidation reaction.

3.1.2. Propylene Epoxidation on Unsupported Ag_{19} and Ag_{20} Clusters. We investigated propylene adsorbing and reacting with a surface oxygen atom to form a PO (epoxidation reaction) on silver clusters. The reaction may involve either the primary (C1) or the secondary (C2) carbon atom of the propylene molecule. The calculated reaction energy profiles of the propylene epoxidation on Ag_{19} and Ag_{20} are shown in Figure 2. A comparison of the C1 and the C2 pathways of Ag_{19} shows that the oxametallacycle (OMC) formation barrier of the C1 pathway is 0.22 eV higher than that of the C2; while for the oxide formation step, the C1 barrier is 0.16 eV lower than C2. The reaction energy profile of the C2 pathway on Ag_{20} is very similar to the C2 on Ag_{19}, indicating that on these slightly larger aggregates, the spin is too delocalized to have a significant effect on the reactivities. For all three energy profiles shown, the overall reactions are exothermic with the highest energy points corresponding to the oxide formation.

dx.doi.org/10.1021/cs4009368 | ACS Catal. 2014, 4, 32−39

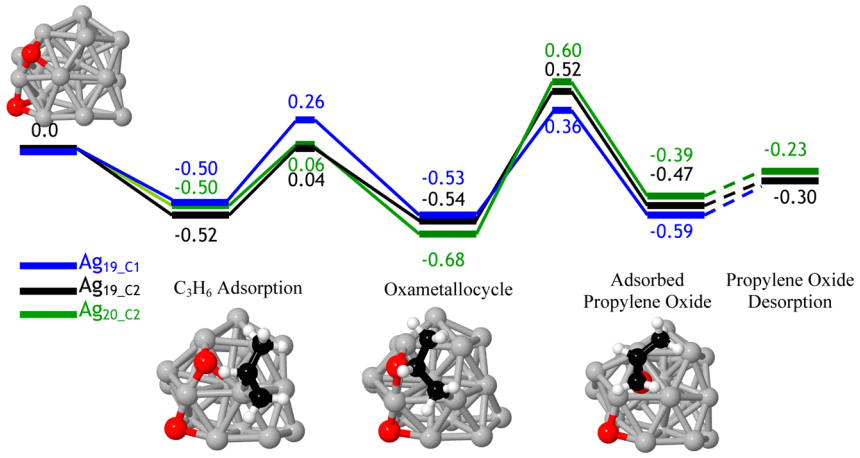

Figure 2. Reaction energy profiles of propylene epoxidation on Ag_{19} and Ag_{20} aggregates, involving either a primary carbon (C1) or a secondary carbon (C2). Energies are in eV. Silver, oxygen, carbon, and hydrogen atoms are shown in silver, red, black, and white, respectively.

3.1.3. O_2 Dissociation and Propylene Epoxidation on Alumina-supported Ag_{19}. The alumina support we used for calculation is an amorphous surface model, as the experimental characterizations of the support indicate. To model the supported Ag_{19}, we first constructed a number of structures by placing the optimized Ag_{19} cluster on top of the amorphous alumina surface, with the largest facet of the cluster interacting with the support surface in different orientations. These structures were then optimized, and the one with the largest binding energy was chosen as the supported Ag_{19} catalyst model. The structure of the Ag_{19} cluster in the supported catalyst model is very similar to that of the gas phase.

Based on experiment[16] there is no evidence for propylene activity on the blank support. Therefore, O_2 dissociation was calculated on two representative sites of the supported Ag_{19} catalyst—a site on top of the Ag aggregate away from the support, referred to as the "top" site, and a site on the interface of the Ag cluster and the alumina support, referred to as the "interfacial" site. The top site we studied is on a pentagonal pyramidal facet, and it is very similar to the most active site for O_2 dissociation on the unsupported Ag_{19}, the "PP neighbor" (Figure 1). The calculated O_2 dissociation reaction energy profile on the top site is shown in Figure 3 in black. The calculated reaction energy of −0.95 eV on the top site is noticeably lower (more exothermic) than on the "PP neighbor" (−0.35 eV); however, the reaction barrier of 0.46 eV is very comparable to that of the "PP neighbor" (0.46 eV). These results suggest that the support does not affect the barriers of O_2 dissociation on Ag sites away from the support. The oxygen atoms in the product of O_2 dissociation on a top site of the Ag cluster are referred to as O_{top}.

The O_2 dissociation on the interfacial site (Figure 3, red), resulting in one oxygen on the Ag cluster ($O_{intf,Ag}$ in Figure 3) and the other on the support, but still bound to the Ag cluster ($O_{intf,s}$ in Figure 3), corresponds to a barrier of 0.16 eV and a reaction energy of −1.80 eV. The barrier and reaction energy are both lower than those of the top site, or any site on the unsupported Ag_{19} (Table 1). Note especially that the intrinsic barrier on the interfacial site is about 0.5 eV lower than that of the top site. This suggests that O_2 dissociation occurs more favorably on the interfacial sites than on top sites. After O_2 dissociation, the two oxygen atoms prefer to stay at two non-neighboring sites, in agreement with the unsupported cluster results. As shown in Figure 3, the $Diss'_{intf}$ and $Diss'_{top}$ structures

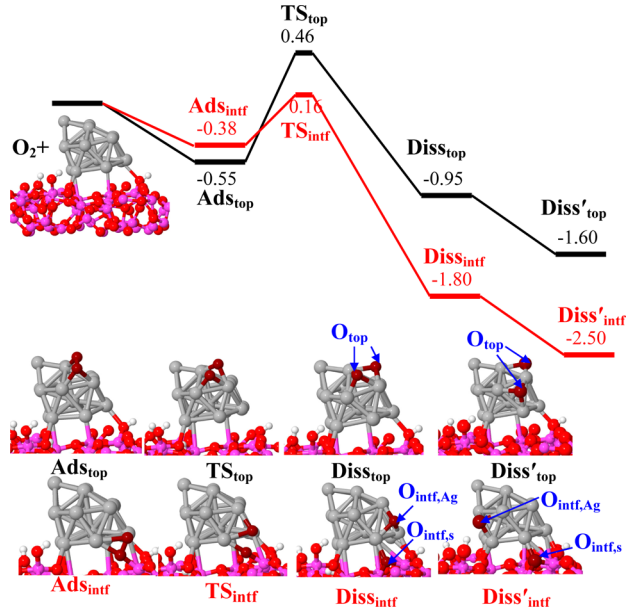

Figure 3. Reaction energy profile of O_2 dissociation on the alumina supported Ag_{19} interfacial (in Red) and top site (in Black). Structures of O_2 adsorption (Ads), dissociation transition state (TS), and product of dissociation (Diss) are shown. More stable structures with two oxygen atoms apart from each other after O_2 dissociation are also shown (Diss′). Silver, oxygen, aluminum, and hydrogen atoms are shown in silver, red, magenta, and white, respectively. The two oxygen atoms from the O_2 molecule are shown in dark red for clarity.

in which two oxygen atoms are on two non-neighboring sites are much lower in energy than the $Diss_{intf}$ and $Diss_{top}$, respectively, where the two oxygen atoms are on neighboring sites.

After O_2 dissociation, there are three types of oxygen sites on the supported silver aggregate to react with propylene: O_{top}, $O_{intf,Ag}$, and $O_{intf,s}$. Propylene epoxidation by an oxygen from the top site O_{top} should have a very similar reaction energy profile to the unsupported aggregate shown in Figure 2 since such sites are far away from, and thus likely to be not affected by, the support. However, the reactivities of the oxygen atoms at the interface, $O_{intf,Ag}$ and $O_{intf,s}$, are different from these on the unsupported Ag_{19}. The $O_{intf,Ag}$ site is bound to the Ag aggregates, and it is active for propylene epoxidation. The

dx.doi.org/10.1021/cs4009368 | ACS Catal. 2014, 4, 32−39

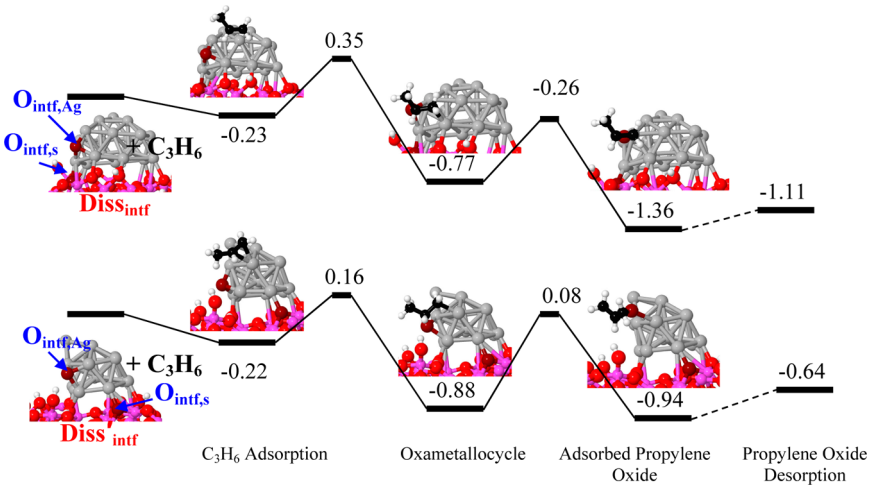

Figure 4. Reaction energy profiles of propylene epoxidation on $O_{intf,Ag}$ sites of $Diss_{intf}$ and $Diss'_{intf}$ structures in Figure 3. Same color code as in Figure 3

epoxidation reactions by the $O_{intf,Ag}$ sites in the $Diss_{intf}$ and $Diss'_{intf}$ structures (Figure 3) are calculated, and the reaction energy profiles are shown in Figure 4. The highest energy points on both pathways correspond to the oxametallocycle formation, in contrast to the results on the unsupported aggregates shown in Figure 2 where the highest energies correspond to oxide formation. The highest energy points in Figure 4 correspond to energies of 0.16 and 0.35 eV, slightly lower than the 0.36 and 0.52 eV (Figure 2) of the highest points on the unsupported Ag_{19}. The overall reactions on the supported Ag_{19} are also more exothermic (−1.11 and −0.64 eV) than those on the unsupported aggregates (−0.30 eV). These results indicate that the epoxidation reaction on a $O_{intf,Ag}$ site is thermodynamically and kinetically more favorable than on an unsupported aggregate. Since we assume that the reactivities of the top sites O_{top} on the supported aggregates are similar to those of the unsupported aggregates, on the alumina-supported Ag aggregate catalyst, both O_{top} and $O_{intf,Ag}$ sites should be active for propylene epoxidation, with the latter being more favorable.

The $O_{intf,s}$ sites, however, are less likely to be very reactive for propylene epoxidation. For example, the $O_{intf,s}$ sites in structure $Diss_{intf}$ and $Diss'_{intf}$ (Figure 3) are sterically hindered to react with a propylene molecule for epoxidation. To demonstrate whether such sites can react with propylene when sterically allowed, we moved the $O_{intf,s}$ in the $Diss'_{intf}$ structure to a more open position while keeping its bond features the same. This new structure is referred to as $Diss''_{intf}$ (Supporting Information, Figure S3). Similar to the $O_{intf,s}$ in $Diss_{intf}$ and $Diss'_{intf}$, the $O_{intf,s}$ in $Diss''_{intf}$ is bound to both the support and the Ag aggregates. We calculated the intermediates of propylene epoxidation by the $O_{intf,s}$ site of $Diss''_{intf}$ (Supporting Information, Figure S3, transition states not calculated), and all intermediate structure energies are much higher than those on O_{top} and $O_{intf,Ag}$ sites. The overall reaction is endothermic by 0.80 eV because the $O_{intf,s}$ is strongly bound to the support. These results indicate that $O_{intf,s}$ sites are most likely not to be active for propylene epoxidation, even if sterically allowed.

3.1.4. Acrolein Formation on Alumina-Supported Ag_{19}. One important issue on using silver as a catalyst for propylene epoxidation is its selectivity toward epoxidation versus the allyl pathway that leads to acrolein formation and combustion. We calculated the reaction barriers for allyl formation (hydrogen abstraction) on O_{top}, $O_{intf,Ag}$, and $O_{intf,s}$ sites. These barriers are lower than those for OMC formation on all three sites (shown in Supporting Information, Figure S4). However, PO was observed to be the dominant product on an alumina supported Ag aggregate catalyst at low reaction temperature in our previous work[16] despite the lower barrier for allyl formation. This is because the acrolein formation and combustion pathways might be limited by the oxygen coverage. CO_2 formation has previously been shown to coincide with acrolein production decrease.[16] The complete acrolein formation pathway involves three steps: first hydrogen abstraction, O transfer to form a formyl group, and the second hydrogen abstraction. Three surface oxygen sites are required to complete the reaction (Scheme 1) since, as shown in our previous work

Scheme 1. Schematic Illustration of Acrolein Formation Involving Three Oxygen Sites

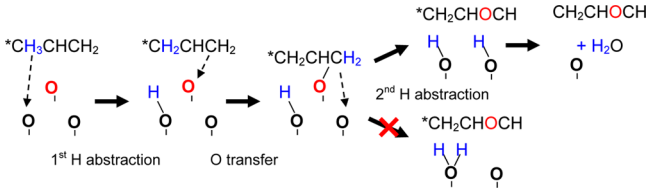

and calculated in this study, the second hydrogen abstraction by the same oxygen as for the first is very endothermic. The combustion of acrolein to form CO_2 requires even more oxygen sites. Therefore, sufficient oxygen coverage is required for acrolein and CO_2 to form. The epoxidation reaction, on the other hand, only requires one oxygen site, and the epoxidation barrier at the interface is low (0.16−0.35 eV) as we calculated. Therefore, the overall selectivity for PO at low temperature is higher than for acrolein or CO_2.

The $O_{intf,s}$ sites, as discussed in previous section, are not likely to be active for epoxidation but can be consumed by the acrolein and combustion pathway since acrolein conversion to CO_2 involves extraction of hydrogen and $O_{intf,s}$ sites are very active for hydrogen abstraction as we have shown in previous and current work. O_{top} and $O_{intf,Ag}$ sites can be active for both epoxide and acrolein pathways. If we compare the ratio of sites that are active for both pathways and sites that are only active for the acrolein pathway, on alumina-supported Ag trimer, this

dx.doi.org/10.1021/cs4009368 | ACS Catal. 2014, 4, 32−39

ratio is $O_{intf,Ag}$:$O_{intf,s}$ (no O_{top} site) and it is roughly 1: 1. These two sites can be replenished by O_2 dissociation at the interface. On alumina-supported Ag aggregates, the additional O_{top} sites are either directly active for epoxidation or they can migrate down to the interface to become (and replenish) $O_{intf,Ag}$ sites (Scheme 2), which are even more active for epoxidation. The ratio of sites for epoxide and acrolein pathways becomes ($O_{intf,Ag}$ + O_{top}):$O_{intf,s}$, and it is higher than the supported trimer. This difference in the sites' ratio might explain why the supported aggregates are more selective for epoxidation than the supported trimers observed experimentally.[16]

Scheme 2. Schematic Illustration of Various Reactions That Occur on the Supported Ag Aggregate

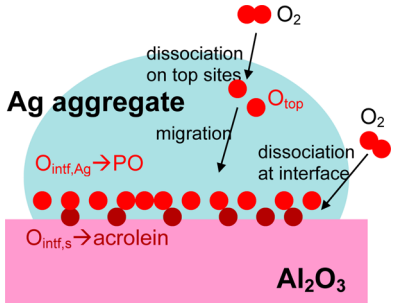

3.2. Experimental Section. *UNCD-Supported Ag_3 Clusters.* To elucidate the role of the alumina support or the cluster/alumina interface, a control experiment was performed, in which the support was carbon based. Size-selected Ag_3 clusters were soft-landed on UNCD, and the sample was treated under a gas mixture of propene and oxygen seeded in helium as applied for the Ag_3/alumina system that eventually led to the formation of ∼2.7 nm tall and ∼3.2 nm diameter aggregates.[16] The aggregation process of UNCD-supported Ag_3 clusters was monitored by in situ GISAXS. The sample was heated up to 500 °C under atmospheric pressure in the gas mixture, to reach the targeted ∼3 nm size for the silver aggregates, comparable with the size of the aggregates obtained on alumina support in previous studies at 200 °C.[16] We assume that the higher temperature needed to reach the final ∼3 nm silver aggregate size on UNCD was due to the strong binding between silver clusters and UNCD defect sites. The horizontal and vertical cuts of the 2-dimensional GISAXS data at select temperatures are plotted in Figure 5a and 5b, respectively. At low temperatures the scatterings are mostly from the roughness of UNCD: the scattering intensity from an object is proportional to the product of the density, the number and the square of the volume of the object. Ag_3 is too small to be detected compared to the mean roughness of UNCD. Therefore, there is no difference in the 25 °C data from the blank UNCD and Ag_3 coated UNCD. Upon heating, the blank UNCD did not show any noticeable roughness change (data are not shown here). The Ag_3 clusters supported on UNCD, however, show significant aggregation during the heat treatment. As the analysis results of the scattering data in Figure 5c and 5d show, the size of Ag particles increases significantly because of the aggregation from 200 °C, and the increase is more along the width (or horizontal) direction at 200 °C, and along both width and height (or vertical direction) at 500 °C.

In contrast to the similar sized silver aggregates on alumina support, no measurable activity was detected on the UNCD-supported aggregates. Since the UNCD support is relatively inert and there is no metal-oxide interface, we expect the reactivities of the UNCD-supported aggregates to be very similar to the unsupported Ag clusters. Because of the lack of interfacial sites, O_2 dissociation and epoxidation are limited on these catalysts. The lack of measurable activity experimentally is in line with our calculation results that the interfacial sites are more active and critical for O_2 dissociation as well as reactions to form epoxide and acrolein.

3.3. Discussion. When a catalytic material is subnanometer sized, its selectivity and activity may deviate from that of the bulk or crystalline surfaces and be determined by various different surface sites and its interface with the support. As our calculations of unsupported Ag clusters show, O_2 dissociation barriers on different sites of Ag clusters range from 0.5 to 2.6 eV. Since the supported Ag aggregate is amorphous and exposes various sites, some sites on the cluster might be active for dissociating O_2 at the reaction conditions. The O_2 dissociation at the Ag/alumina interfacial sites corresponds to a barrier of 0.2 eV, even more favorable than on top sites.

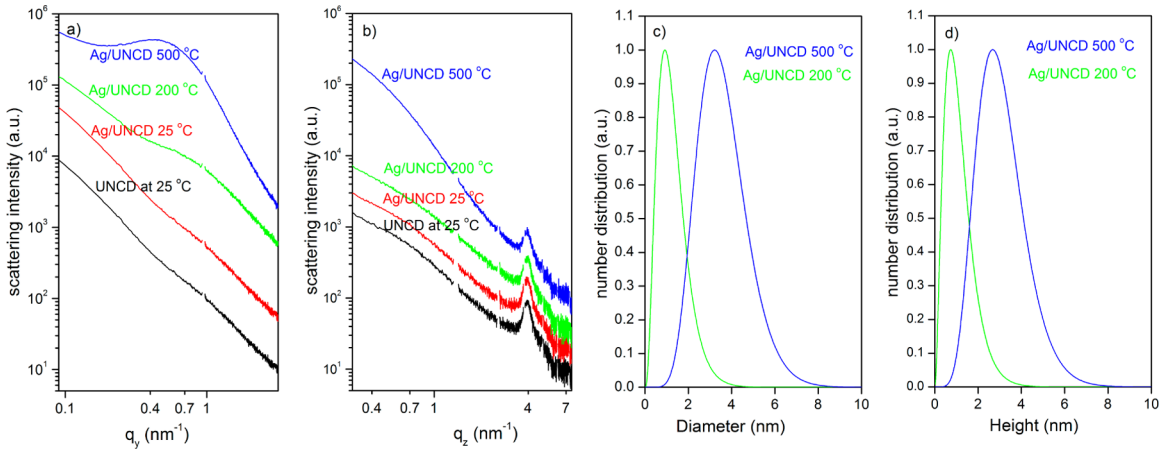

Figure 5. Horizontal (a) and vertical (b) cuts of the 2-dimensional GISAXS data of UNCD-supported silver clusters at selected temperatures of 25 °C, 200 °C, and 500 °C during the assembly process. As reference, the GISAXS cuts for the blank UNCD supports are shown as well. The apparent peak at ∼4 nm^{-1} arises from scattering by the Kapton window of the in situ cell. Plots in (c) and (d) show the horizontal and vertical size distributions of the silver aggregates at 200 and 500 °C obtained from the analysis of the GISAXS cuts shown in (a) and (b), respectively.

dx.doi.org/10.1021/cs4009368 | ACS Catal. 2014, 4, 32−39

Therefore, we expect more dissociated oxygen at the interface than on top sites. These barriers for oxygen dissociation on the aggregates are also small compared to crystalline surfaces, which indicates that availability of oxygen will not be a rate limiting step for epoxidation on the aggregates as in the case of the crystalline surfaces.[14]

We summarize the reactions on the supported silver aggregate in Scheme 2. As our calculations show, $O_{intf,Ag}$ sites, as products of O_2 dissociation at interfacial sites, are thermodynamically and kinetically active for propylene epoxidation (exothermic with a barrier of 0.16−0.35 eV). The noninterfacial sites, such as O_{top} or sites on unsupported Ag cluster, are less active. However, O_{top} sites can migrate to the interfacial sites (thermodynamically favored and kinetically fast) to replenish $O_{intf,Ag}$ sites and react with propylene to form PO, as illustrated in Scheme 2. Therefore, the interface between Ag aggregate and the oxide support is likely to be the most reactive center of the subnanometer silver/alumina catalysts and is consistent with the high activity observed experimentally at low temperatures.[16] This origin of high catalytic activity from special active sites at the metal and oxide interface has also been highlighted in the literature.[36−52]

The allyl pathways on all three types of sites correspond to lower reaction barriers than the selective epoxidation pathways. However, to complete the reaction to produce the final products acrolein or CO_2 requires multiple oxygen sites close to the molecule adsorption sites. Therefore, the allyl pathways do not prevail despite the low reaction barriers. These reactions are more likely to occur also at the interface because the oxygen coverage is relatively higher at these positions. Although we have not explicitly studied the O coverage effect on reaction mechanisms, it has been shown in the literature that the barrier of epoxidation reaction decreases and exothermicity increases when the O coverage increases.[53] This trend is probably because as the coverage increases, the binding of O to the surface becomes weaker so the site becomes more active. Therefore, as the O coverage increases, the rates of both the nonselective acrolein/combustion and the selective epoxidation increase—the former is due to more O sites availability, the latter is due to both more O sites availability and reduced barrier. The lack of measurable activity of the Ag/UNCD catalyst also is consistent with the lower activity of the top sites relative to the interfacial sites: the UNCD support is expected to provide less reactive interfacial sites with silver aggregates for O_2 dissociation or propylene epoxidation in comparison to the interface in the case of alumina-supported aggregates.

The results presented in this study using a more realistic amorphous alumina model as the support are in qualitative agreement with those calculated with a θ-alumina support model as used in our previous study. For example, the conclusion that O_2 dissociation is more favorable at the interfacial sites than on top sites and that the $O_{intf,Ag}$ sites are active but $O_{intf,s}$ sites are not active for propylene epoxidation can be drawn from calculations using both models.

4. CONCLUSIONS

Oxygen dissociation and propylene epoxidation reactions were studied on unsupported Ag_{19} and Ag_{20} clusters, as well as alumina-supported Ag_{19} using DFT. Our calculations show that the O_2 dissociation at the interface between the Ag aggregate and the alumina support is more favorable than on sites away from the interface. After O_2 dissociation at the interface, the oxygen on the Ag aggregate ($O_{intf,Ag}$) is mainly active for propylene epoxidation, while the oxygen on the support ($O_{intf,s}$) is mainly responsible for the acrolein formation and combustion. The epoxidation reaction is also more favorable at the $O_{intf,Ag}$ sites than on oxygen sites away from the interface (O_{top}). Thus, the mechanism at the interface is similar to what we found for the silver trimer on alumina[16] and can account for the high activity observed for the direct oxidation of propylene on the Ag aggregates.[16] In addition, the barriers for oxygen dissociation on these model systems both at the interface and on the surfaces are small compared to that on crystalline surfaces, which indicates that availability of oxygen will not be a rate limiting step for the epoxidation reaction on the aggregates as in the case of the crystalline surfaces. This accounts for the increased activity of the aggregates compared to the silver crystalline surfaces.

The assembly of UNCD-supported silver trimers into small nanometer size aggregates under reactive conditions of propylene partial oxidation was also investigated experimentally. The UNCD-supported Ag clusters were found to be not measurably active toward propylene oxidation. This observation confirms the role of the metal-oxide interfacial sites on the alumina-supported nanoscale aggregates as the active center where the metal-oxide interfacial sites both promote oxygen dissociation and reduce propylene epoxidation barriers. This is believed to be responsible for the high observed propylene oxidation activity compared to the UNCD supported aggregates.

Thus, this combined computational and experimental study shows that the metal-oxide interface as well as the noncrystalline surfaces of the silver aggregates on alumina supports plays an important role in promoting the propylene epoxidation catalytic reaction occurring on them.

■ ASSOCIATED CONTENT

Supporting Information

Structures of O_2 dissociation transition states and products on various sites of Ag_{19}; reaction energy profiles of O migrating from a neighboring to a non-neighboring site on the Ag_{19} and Ag_{20} clusters; reaction intermediates for propylene epoxidation on a $O_{intf,s}$ site of structure $Diss''_{intf}$, reaction energies and barriers of the first hydrogen abstraction (allyl pathway) from propylene by $O_{intf,Ag}$, $O_{intf,s}$, and O_{top} sites; Al K-edge X-ray absorption spectra of the amorphous alumina deposited onto a Si wafer shown together with reference materials. This material is available free of charge via the Internet at http://pubs.acs.org.

■ AUTHOR INFORMATION

Corresponding Author

*E-mail: curtiss@anl.gov.

Notes

The authors declare no competing financial interest.

■ ACKNOWLEDGMENTS

This work was supported by BES-Materials Sciences and use of the Advanced Photon Source, an Office of Science User Facility operated for the U.S. Department of Energy (DOE) Office of Science by Argonne National Laboratory, was supported by the U.S. DOE under Contract No. DE-AC02-06CH11357. J.G. acknowledges a DOE Early Career Award from the Office of Science, Office of Basic Energy Sciences, Chemical Sciences Division. The authors acknowledge the use of Argonne Advanced Photon Source (the 12-ID-B beamline) and Michael

Hävecker for providing some reference Al K-edge spectra. The computational work was performed using facilities of the Center for Nanoscale Materials and Laboratory Computing Resource Center at Argonne, and EMSL located at Pacific Northwest National Laboratory.

REFERENCES

(1) Hayashi, T.; Tanaka, K.; Haruta, M. *J. Catal.* **1998**, *178*, 566−575.
(2) Lambert, R. M.; Williams, F. J.; Cropley, R. L.; Palermo, A. *J. Mol. Catal. A: Chem.* **2005**, *228*, 27−33.
(3) Lu, J. Q.; Bravo-Suarez, J. J.; Takahashi, A.; Haruta, M.; Oyama, S. T. *J. Catal.* **2005**, *232*, 85−95.
(4) Luo, M. F.; Lu, J. Q.; Li, C. *Catal. Lett.* **2003**, *86*, 43−49.
(5) Nijhuis, T. A. R.; Visser, T.; Weckhuysen, B. M. *Angew. Chem., Int. Ed.* **2005**, *44*, 1115−1118.
(6) Yao, W.; Guo, Y. L.; Liu, X. H.; Guo, Y.; Wang, Y. Q.; Wang, Y. S.; Zhang, Z. G.; Lu, G. Z. *Catal. Lett.* **2007**, *119*, 185−190.
(7) Zemichael, F. W.; Palermo, A.; Tikhov, M. S.; Lambert, R. M. *Catal. Lett.* **2002**, *80*, 93−98.
(8) Serafin, J. G.; Liu, A. C.; Seyedmonir, S. R. *J. Mol. Catal. A: Chem.* **1998**, *131*, 157−168.
(9) Barteau, M. A.; Madix, R. J. *J. Am. Chem. Soc.* **1983**, *105*, 344−349.
(10) Torres, D.; Lopez, N.; Illas, F.; Lambert, R. M. *Angew. Chem., Int. Ed.* **2007**, *46*, 2055−2058.
(11) Linic, S.; Barteau, M. A. *J. Am. Chem. Soc.* **2003**, *125*, 4034−4035.
(12) Linic, S.; Barteau, M. A. *J. Catal.* **2003**, *214*, 200−212.
(13) Kulkarni, A.; Bedolla-Pantoja, M.; Singh, S.; Lobo, R. F.; Mavrikakis, M.; Barteau, M. A. *Top. Catal.* **2012**, *55*, 3−12.
(14) Pulido, A.; Concepcion, P.; Boronat, M.; Corma, A. *J. Catal.* **2012**, *292*, 138−147.
(15) Molina, L. M.; Lee, S.; Sell, K.; Barcaro, G.; Fortunelli, A.; Lee, B.; Seifert, S.; Winans, R. E.; Elam, J. W.; Pellin, M. J.; Barke, I.; von Oeynhausen, V.; Lei, Y.; Meyer, R. J.; Alonso, J. A.; Rodriguez, A. F.; Kleibert, A.; Giorgio, S.; Henry, C. R.; Meiwes-Broer, K. H.; Vajda, S. *Catal. Today* **2011**, *160*, 116−130.
(16) Lei, Y.; Mehmood, F.; Lee, S.; Greeley, J.; Lee, B.; Seifert, S.; Winans, R. E.; Elam, J. W.; Meyer, R. J.; Redfern, P. C.; Teschner, D.; Schlogl, R.; Pellin, M. J.; Curtiss, L. A.; Vajda, S. *Science* **2010**, *328*, 224−228.
(17) Adiga, S. P.; Zapol, P.; Curtiss, L. A. *Phys. Rev. B* **2006**, *74*, 064204.
(18) Adiga, S. P.; Zapol, P.; Curtiss, L. A. *J. Phys. Chem. C* **2007**, *111*, 7422−7429.
(19) Lee, S. K.; Park, S. Y.; Yi, Y. S.; Moon, J. *J. Phys. Chem. C* **2010**, *114*, 13890−13894.
(20) Lizarraga, R.; Holmstrom, E.; Parker, S. C.; Arrouvel, C. *Phys. Rev. B* **2011**, *83*, 094201.
(21) Lamparter, P.; Kniep, R. *Phys. B* **1997**, *234*, 405−406.
(22) Perdew, J. P.; Wang, Y. *Phys. Rev. B* **1992**, *45*, 13244−13249.
(23) Kresse, G.; Furthmuller, J. *Phys. Rev. B* **1996**, *54*, 11169−11186.
(24) Kresse, G.; Furthmuller, J. *Comput. Mater. Sci.* **1996**, *6*, 15−50.
(25) Kresse, G.; Hafner, J. *Phys. Rev. B* **1993**, *47*, 558−561.
(26) Kresse, G.; Hafner, J. *Phys. Rev. B* **1994**, *49*, 14251−14269.
(27) Carlisle, J.; Advanced Diamond Technologies, Inc.; http://www.thindiamond.com/index.php?cID=145.
(28) Lee, S.; Di Vece, M.; Lee, B.; Seifert, S.; Winans, R. E.; Vajda, S. *Phys. Chem. Chem. Phys.* **2012**, *14*, 9336−9342.
(29) Lee, S.; Lee, B.; Seifert, S.; Vajda, S.; Winans, R. E. *Nucl. Instrum. Methods Phys. Res., Sect. A* **2011**, *649*, 200−203.
(30) Lee, S.; Molina, L. M.; Lopez, M. J.; Alonso, J. A.; Hammer, B.; Lee, B.; Seifert, S.; Winans, R. E.; Elam, J. W.; Pellin, M. J.; Vajda, S. *Angew. Chem., Int. Ed.* **2009**, *48*, 1467−1471.
(31) Wyrzgol, S. A.; Schafer, S.; Lee, S.; Lee, B.; Di Vece, M.; Li, X. B.; Seifert, S.; Winans, R. E.; Stutzmann, M.; Lercher, J. A.; Vajda, S. *Phys. Chem. Chem. Phys.* **2010**, *12*, 5585−5595.
(32) Ferguson, G. A.; Yin, C. R.; Kwon, G.; Tyo, E. C.; Lee, S.; Greeley, J. P.; Zapol, P.; Lee, B.; Seifert, S.; Winans, R. E.; Vajda, S.; Curtiss, L. A. *J. Phys. Chem. C* **2012**, *116*, 24027−24034.
(33) Lee, S.; Di Vece, M.; Lee, B.; Seifert, S.; Winans, R. E.; Vajda, S. *ChemCatChem* **2012**, *4*, 1632−1637.
(34) http://usaxs.xray.aps.anl.gov/staff/ilavsky/irena.html.
(35) Zhao, J.; Luo, Y.; Wang, G. *Eur. Phys. J. D* **2001**, *14*, 309−316.
(36) Janssens, T. V. W.; Clausen, B. S.; Hvolbaek, B.; Falsig, H.; Christensen, C. H.; Bligaard, T.; Norskov, J. K. *Top. Catal.* **2007**, *44*, 15−26.
(37) Okumura, M.; Nakamura, S.; Tsubota, S.; Nakamura, T.; Azuma, M.; Haruta, M. *Catal. Lett.* **1998**, *51*, 53−58.
(38) Liu, Z. P.; Hu, P.; Alavi, A. *J. Am. Chem. Soc.* **2002**, *124*, 14770−14779.
(39) Schubert, M. M.; Hackenberg, S.; van Veen, A. C.; Muhler, M.; Plzak, V.; Behm, R. J. *J. Catal.* **2001**, *197*, 113−122.
(40) Molina, L. M.; Hammer, B. *Phys. Rev. Lett.* **2003**, *90*, 206102.
(41) Molina, L. M.; Hammer, B. *Phys. Rev. B* **2004**, *69*, 155424.
(42) Molina, L. M.; Rasmussen, M. D.; Hammer, B. *J. Chem. Phys.* **2004**, *120*, 7673−7680.
(43) Molina, L. M.; Hammer, B. *Appl. Catal., A* **2005**, *291*, 21−31.
(44) Sakurai, H.; Akita, T.; Tsubota, S.; Kiuchi, M.; Haruta, M. *Appl. Catal., A* **2005**, *291*, 179−187.
(45) Bond, G. C.; Thompson, D. T. *Gold Bull.* **2000**, *33*, 41−51.
(46) Mudiyanselage, K.; Senanayake, S. D.; Feria, L.; Kundu, S.; Baber, A. E.; Graciani, J.; Vidal, A. B.; Agnoli, S.; Evans, J.; Chang, R.; Axnanda, S.; Liu, Z.; Sanz, J. F.; Liu, P.; Rodriguez, J. A.; Stacchiola, D. J. *Angew. Chem., Int. Ed.* **2013**, *52*, 5101−5105.
(47) Hayek, K.; Kramer, R.; Paal, Z. *Appl. Catal., A* **1997**, *162*, 1−15.
(48) Rodriguez, J. A.; Evans, J.; Graciani, J.; Park, J. B.; Liu, P.; Hrbek, J.; Sanz, J. F. *J. Phys. Chem. C* **2009**, *113*, 7364−7370.
(49) Valero, M. C.; Raybaud, P.; Sautet, P. *J. Phys. Chem. B* **2006**, *110*, 1759−1767.
(50) Valero, M. C.; Raybaud, P.; Sautet, P. *J. Catal.* **2007**, *247*, 339−355.
(51) Guzman, J.; Carrettin, S.; Fierro-Gonzalez, J. C.; Hao, Y. L.; Gates, B. C.; Corma, A. *Angew. Chem., Int. Ed.* **2005**, *44*, 4778−4781.
(52) Concepcion, P.; Corma, A.; Silvestre-Albero, J.; Franco, V.; Chane-Ching, J. Y. *J. Am. Chem. Soc.* **2004**, *126*, 5523−5532.
(53) Ozbek, M. O.; Onal, I.; van Santen, R. A. *Top. Catal.* **2012**, *55*, 710−717.